AIAA JOURNAL
Vol. 39, No. 6, June 2001

Thermopiezoelastic Snapping of Piezolaminated Plates Using Layerwise Nonlinear Finite Elements

Il-Kwon Oh,* Jae-Hung Han,† and In Lee‡
Korea Advanced Institute of Science and Technology, Taejon 305-701, Republic of Korea

The thermopiezoelastic snapping phenomena of piezolaminated plates are numerically simulated by applying a cylindrical arc-length scheme to Newton–Raphson method. Based on the layerwise displacement theory and von Kármán strain-displacement relationships, nonlinear finite element formulations are derived for thermopiezoelastic composite plates. From the static and dynamic viewpoint, nonlinear thermopiezoelastic behavior and vibration characteristics are investigated for symmetric and eccentric structural models with various piezoelectric actuation modes. Present results show the possibility to enhance the performance of thermal structures using piezoelectric actuators and report new phenomena, namely thermopiezoelastic snapping, induced by the excessive piezoelectric actuation in the active suppression of thermally buckled large deflection of piezolaminated plates.

Nomenclature

a, b	=	panel length, width
c	=	maximum thickness of plate
c_{base}	=	thickness of base composite
$\boldsymbol{D}_k$	=	electric displacement vector
$\boldsymbol{E}_k$	=	electric field vector
e_{kj}	=	piezoelectric coefficient
f_i	=	volume force
K	=	kinetic energy
$p_k^{S,E}$	=	pyroelectric constant
$Q_{ij}^{E,\Delta T}$	=	elastic moduli
T_i	=	surface traction
t_0	=	arbitrary time
U	=	strain energy
U^J, V^J	=	in-plane displacements
V	=	work done by external force
$\alpha_i^{S,E}$	=	thermal expansion coefficient
$\Delta T_{\text{cr},G}^{\text{SF(EF)}}$	=	thermal buckling temperature of symmetrically and fully covered piezolaminated plate (SF) [eccentrically and fully covered piezolaminated plate (EF)] structural model under grounding state
ΔT_k	=	temperature rise in kth layer
δ	=	virtual quantity
$\varepsilon_{kl}^{S,\Delta T}$	=	dielectric constant
ε_j	=	strain vector
ρ	=	density of materials
σ_i	=	stress vector
$\Phi^J(z)$	=	linear Lagrangian interpolation

Subscripts and Superscript

e	=	finite elements
G	=	grounding
L	=	lower piezoactuator
U	=	upper piezoactuator
$\bullet$	=	time derivative

Introduction

THE development of adaptive materials and their applications in smart and intelligent structures have opened a new way to structural engineering. Among several functional materials, piezoelectric materials have drawn attention for the enhancement of structural performance via buckling and shape control and noise and vibration suppression. Even though numerous studies on the modeling and analysis of piezolaminated composite structures have been performed, nonlinear thermopiezoelastic analyses are still rare. This paper reports thermopiezoelastic snapping phenomena of laminated composite plates with surface bonded piezoelectric actuators induced by thermal and electric loads.

Mathematical modeling on piezoelectric composite beams, plates, and shells has been studied based on classical and other equivalent single-layer theories by many researchers including Crawley and de Luis,[1] Wang and Rogers,[2] Lee,[3] Tzou and Tseng,[4] and Han and Lee.[5] Recently, discrete layer theories have been utilized for the analysis of composite beam,[6,7] plate,[8,9] and shell[10] structures with piezoelectric layers to consider fully the effects of transverse shear and variable in-plane displacements through the thickness. Most studies on smart structures using piezoelectric materials are aimed at vibration and static shape controls. Also, the applications of piezoelectric actuators to bucking control are found in several studies. Meressi and Paden[11] designed a linear quadratic regulator controller for the effective buckling control of a beam. Thompson and Loughlan[12] performed an experimental study on the active bucking control of a column with surface bonded piezoelectric materials. Faria and Almeida[13] investigated the enhancement of prebuckling behavior of composite beams with geometric imperfections using piezoelectric actuators.

Because high-speed aircraft, rocket, and launch vehicles are subject to severe thermal environments, as well as aerodynamic loads, thermal effects on the structural components should be taken into account. Thermal stresses due to aerodynamic heating may induce buckling and dynamic instability of the aerospace structures. Literature can be found on the linear analysis of piezolaminated composites under the thermal environment. Ha et al.[14] investigated a shape control to minimize the transverse deflection of thermally distorted panels due to thermal gradients using an eight-node three-dimensional composite brick element. Tzou and Ye[15] developed a new three-dimensional finite element and analyzed thermal influences on the sensing and control of piezoelectric/steel laminates. Lee and Saravanos[16] formulated linear finite element equations for multilayered thermal piezoelectric composite plates with layerwise generalization to capture locally induced piezoelectric and thermal effects. Smittakorn and Heyliger[17] investigated the steady state and transient behavior of laminated hygrothermopiezoelastic plates under the coupled effects of mechanical, electrical, thermal, and moisture fields using a three-dimensional discrete-layer model.

However, skin panels of space shuttles and high-speed flight vehicles may experience large deflections due to thermal postbuckling. Because conventional aircraft structural components are often designed to operate in the postbuckling range, it is very important

Received 16 January 2000; revision received 30 November 2000; accepted for publication 19 December 2000.

*Graduate Research Assistant, Department of Aerospace Engineering.
†Postdoctoral Fellow, Department of Aerospace Engineering; currently Senior Researcher, Satellite Communication Payload Team, Electronics and Telecommunications Research Institute, 161 Kajong-Dong, Yusong-Gu, Taejon 305-350, Republic of Korea.
‡Professor, Department of Aerospace Engineering. Senior Member AIAA.

to study the effect of geometric nonlinearities and to analyze the nonlinear static and dynamic behaviors of composite structures. Babero and Reddy[18] formulated a geometrically nonlinear layerwise displacement theory to consider effectively the transverse shear effect and cross-sectional warping. Pai et al.[19] presented a refined geometric nonlinear model of composite plates with integrated piezoelectric actuators and sensors. Tzou and Zhou[20] and Bao et al.[21] proposed a mathematical modeling of nonlinear thermopiezoelastic laminates and investigated the static and dynamic control of beams, plates, and shells. Oh et al.[22] performed postbuckling and vibration analyses considering large thermal deflections for fully and partially covered piezolaminated composite plates.

A literature survey shows that thermopiezoelastic buckling and postbuckled behavior of composite plates with active piezoelectric layers are still unexplored. In this paper, the thermopiezoelastic snapping phenomena of piezolaminated plates are numerically simulated using cylindrical arc-length scheme[23] applied to Newton–Raphson method. The nonlinear finite element equations based on the layerwise plate theory and von Kármán strain-displacement relationships are developed for a piezolaminated composite plate subject to thermomechanical and piezoelectric loads. The assembled finite element equations can be divided into two coupled equations: the nonlinear time-independent equation for static prebuckling and postbuckling equilibrium states and the linear time-dependent equation for small vibrations about these equilibrium points. Numerical results are presented for symmetric and eccentric structural models with various actuation modes. Generally, snapping phenomena, which are unstable postbuckling behaviors with sudden reduction of the load carrying capacity, have been reported for curved panels,[24] whereas it is believed that the postbuckling behavior of flat panels is stable. The present results show that postbuckled deflections due to compressive in-plane thermal stresses may not be successfully suppressed in some actuation modes because of thermopiezoelastic snap-through phenomena, whereas a large deflection due to transverse loading such as surface pressure can be efficiently reduced by out-of-phase actuation mode.

Layerwise Nonlinear Finite Element Formulation

Based on the partial layerwise plate theory,[18] the displacement fields (u_1, u_2, and u_3) for a two-dimensional element i, of which area is defined as Ω_i, can be expressed as shown in Eq. (1) by introducing the piecewise interpolation function $\Phi^J(z)$:

$$u_1 = \sum_{J=1}^{N_i} U^J(x, y, t)\Phi^J(z), \qquad u_2 = \sum_{J=1}^{N_i} V^J(x, y, t)\Phi^J(z)$$
$$u_3 = W(x, y, t) \tag{1}$$

where, u_1, u_2, and u_3 are the displacements in the x, y, and z directions, respectively. The displacement-based partial layerwise theory provides a more realistic description of the kinematics of composite laminates when compared to the equivalent single-layer theories by introducing zigzag behavior of the in-plane displacements. In this study, the partial layerwise theory is applied for the modeling of thermopiezoelastic plates, though the full layerwise theory[8,25] will give more accurate solutions for the thick plates by adding discrete-layer transverse normal effects.

The von Kármán nonlinear strain-displacement relationship is adopted to consider a large deflection due to thermopiezoelectric loads. The relationship between strain and displacement can be written as

$$\varepsilon_x = \frac{\partial u_1}{\partial x} + \frac{1}{2}\left(\frac{\partial u_3}{\partial x}\right)^2 = \sum_{J=1}^{N_i} \frac{\partial U^J}{\partial x}\Phi^J + \frac{1}{2}\left(\frac{\partial W}{\partial x}\right)^2 \tag{2a}$$

$$\varepsilon_y = \frac{\partial u_2}{\partial y} + \frac{1}{2}\left(\frac{\partial u_3}{\partial y}\right)^2 = \sum_{J=1}^{N_i} \frac{\partial V^J}{\partial y}\Phi^J + \frac{1}{2}\left(\frac{\partial W}{\partial y}\right)^2 \tag{2b}$$

$$\gamma_{xy} = \frac{\partial u_1}{\partial y} + \frac{\partial u_2}{\partial x} + \frac{\partial u_3}{\partial x}\frac{\partial u_3}{\partial y}$$
$$= \sum_{J=1}^{N_i}\left(\frac{\partial U^J}{\partial y} + \frac{\partial V^J}{\partial x}\right)\Phi^J + \frac{\partial W}{\partial x}\frac{\partial W}{\partial y} \tag{2c}$$

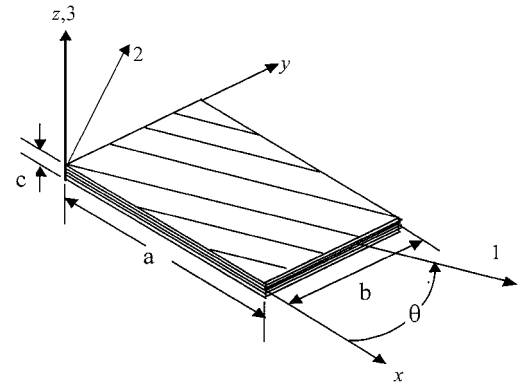

Fig. 1 Geometry and coordinate systems of base laminated plates.

$$\gamma_{yz} = \frac{\partial u_3}{\partial y} + \frac{\partial u_2}{\partial z} = \frac{\partial W}{\partial y} + \sum_{J=1}^{N_i} V^J \frac{\mathrm{d}\Phi^J}{\mathrm{d}z} \tag{2d}$$

$$\gamma_{xz} = \frac{\partial u_3}{\partial x} + \frac{\partial u_1}{\partial z} = \frac{\partial W}{\partial x} + \sum_{J=1}^{N_i} U^J \frac{\mathrm{d}\Phi^J}{\mathrm{d}z} \tag{2e}$$

The linear constitutive equations[26] of the kth layer for a thermopiezoelastic material can be written as

$$\sigma_i = Q_{ij}^{E,\Delta T}\varepsilon_j - e_{ki}E_k - \alpha_i^{S,E}\Delta T_k \tag{3}$$

$$D_k = e_{kj}\varepsilon_j + \varepsilon_{kl}^{S,\Delta T}E_l + p_k^{S,E}\Delta T_k \tag{4}$$

Material degradation due to temperature increase is neglected. The constitutive equation in the geometric x–y–z coordinate system shown in Fig. 1 can be obtained by the proper coordinate transformation.[22]

For the modeling of actuation problems only, because the variations of electric fields components are zero and electric charge are often not considered, a variational thermopiezoelastic equation with a linear potential assumption can be obtained by using conventional Hamilton's principle, so-called thermal analogy approach,[27] in the following form:

$$\delta\Pi = \delta(U + V) - \delta K$$
$$= \int_0^{t_0}\left\{\int_V (\sigma_i\delta\varepsilon_i - f_i\delta u_i - \rho\ddot{u}_i\delta\dot{u}_i)\,\mathrm{d}V - \int_S T_i\delta u_i\,\mathrm{d}S\right\}\mathrm{d}t$$
$$= 0 \tag{5}$$

However, fully thermopeizoelastic coupled formulations will give a more accurate result by considering induced electric potentials and pyroelectricity.

The nonlinear finite element equation for each element can be obtained by introduction of Lagrangian shape functions as follows:

$$\boldsymbol{M}_e\ddot{\boldsymbol{u}}_e + \left(\boldsymbol{K0}_e - \boldsymbol{K}_e^{\Delta T} - \boldsymbol{K}_e^P + \tfrac{1}{2}\boldsymbol{KN1}_e + \tfrac{1}{3}\boldsymbol{KN2}_e\right)\boldsymbol{u}_e = \boldsymbol{F}_e^{\Delta T} + \boldsymbol{F}_e^P \tag{6}$$

where $\boldsymbol{M}_e$, $\boldsymbol{K0}_e$, $\boldsymbol{K}_e^{\Delta T}$, $\boldsymbol{K}_e^P$, $\boldsymbol{KN1}_e$, $\boldsymbol{KN2}_e$, $\boldsymbol{F}_e^{\Delta T}$, and $\boldsymbol{F}_e^P$ are mass matrix, linear stiffness, thermal geometric stiffness, piezoelectric geometric stiffness, first-order nonlinear stiffness, second-order nonlinear stiffness, thermal load vector, and piezoelectric force vectors, respectively. The detailed derivations and expressions of Eq. (6) may be found in our previous study.[22]

Solution Scheme for Thermopiezoelastic Nonlinear Behavior

Through the assembly procedure, the global nonlinear finite element equation can be obtained as follows:

$$\boldsymbol{M}\ddot{\boldsymbol{u}} + \left(\boldsymbol{K0} - \boldsymbol{K}^{\Delta T} - \boldsymbol{K}^P + \tfrac{1}{2}\boldsymbol{KN1} + \tfrac{1}{3}\boldsymbol{KN2}\right)\boldsymbol{u} = \boldsymbol{F}^{\Delta T} + \boldsymbol{F}^P \tag{7}$$

To analyze the thermopiezoelastic deformation and vibration characteristics of piezolaminated plates subject to thermopiezoelectric loads, the solution of Eq. (7) is assumed to be the sum of a time-dependent and a time-independent solution, $\boldsymbol{u} = \boldsymbol{u}_s + \boldsymbol{u}_t$, where $\boldsymbol{u}_s$ is the static large deflection and $\boldsymbol{u}_t$ is the time-dependent solution with small amplitude. Substituting this assumed displacement into Eq. (7) and using the transformation such as $\boldsymbol{KN1}(\boldsymbol{u}_t)\boldsymbol{u}_s = \boldsymbol{KN1}(\boldsymbol{u}_s)\boldsymbol{u}_t$, we can obtain static and dynamic coupled equations:

$$\left[\boldsymbol{K0} - \boldsymbol{K}^{\Delta T} - \boldsymbol{K}^{P} + \tfrac{1}{2}\boldsymbol{KN1}(\boldsymbol{u}_s) + \tfrac{1}{3}\boldsymbol{KN2}(\boldsymbol{u}_s)\right]\boldsymbol{u}_s = \boldsymbol{F}^{\Delta T} + \boldsymbol{F}^{P} \tag{8}$$

$$\boldsymbol{M}\ddot{\boldsymbol{u}}_t + \left[\boldsymbol{K0} - \boldsymbol{K}^{\Delta T} - \boldsymbol{K}^{P} + \boldsymbol{KN1}(\boldsymbol{u}_s) + \boldsymbol{KN2}(\boldsymbol{u}_s)\right]\boldsymbol{u}_t = 0 \tag{9}$$

Solution Procedure for Thermal Buckling and Postbuckling

Thermal Euler buckling analysis is performed to find a thermal buckling temperature rise ΔT_{cr} using the following equation:

$$\left(\boldsymbol{K0} - \Delta T_{\mathrm{cr}}\boldsymbol{K}_0^{\Delta T}\right)\{\Theta\} = \boldsymbol{0} \tag{10}$$

where $\boldsymbol{K}_0^{\Delta T}$ is the geometric stiffness in the state of unit uniform temperature distribution and $\{\Theta\}$ is the thermal buckling mode. The fundamental buckling mode shape is properly scaled as an initial estimated deflection in the construction of nonlinear stiffness matrix in the postbuckled range.

The Newton–Raphson iteration method is used to solve the thermoelastic postbuckling problem. For the $(i+1)$th iteration, an incremental equation can be written from Eq. (8) without piezoelectric terms as follows:

$$\left[\boldsymbol{K0} - \boldsymbol{K}^{\Delta T} + \boldsymbol{KN1}\left(\boldsymbol{u}_s^i\right) + \boldsymbol{KN2}\left(\boldsymbol{u}_s^i\right)\right]\Delta\boldsymbol{u}_s^{i+1} = \Delta\boldsymbol{F}^i \tag{11}$$

where

$$\Delta\boldsymbol{F}^i = \boldsymbol{F}^{\Delta T} - \left[\boldsymbol{K0} - \boldsymbol{K}^{\Delta T} + \tfrac{1}{2}\boldsymbol{KN1}\left(\boldsymbol{u}_s^i\right) + \tfrac{1}{3}\boldsymbol{KN2}\left(\boldsymbol{u}_s^i\right)\right]\boldsymbol{u}_s^i \tag{12}$$

When Eq. (11) is solved, the updated displacement vector is determined as follows:

$$\boldsymbol{u}_s^{i+1} = \boldsymbol{u}_s^i + \Delta\boldsymbol{u}_s^{i+1} \tag{13}$$

where $\boldsymbol{u}_s^{i+1}$ and $\Delta\boldsymbol{u}_s^{i+1}$ are the static and incremental displacement in the $(i+1)$th iteration.

Solution Procedure for Thermopiezoelastic Snapping

The suppression of thermomechanical large deflections of piezolaminated plates using piezoelectric actuators may induce snapping phenomena. In our previous study,[22] we did not make a close examination of the nonlinear characteristics of piezolaminated plates including snap-through phenomena. To analyze a snapping process, we incorporated the cylindrical arc-length scheme[23] with the Newton–Raphson iteration method in this study. The out-of-balance vector $\boldsymbol{q}$ of a thermopiezoelastic system is defined by piezoelectric load level λ_P under a given temperature field:

$$\boldsymbol{q}(\boldsymbol{u}_s, \lambda_P) = \left[\boldsymbol{K0} - \boldsymbol{K}^{\Delta T} - \lambda_P\boldsymbol{K}_0^{P} + \tfrac{1}{2}\boldsymbol{KN1}(\boldsymbol{u}_s) + \tfrac{1}{3}\boldsymbol{KN2}(\boldsymbol{u}_s)\right]\boldsymbol{u}_s - \lambda_P\boldsymbol{F}_0^{P} - \boldsymbol{F}^{\Delta T} = 0 \tag{14}$$

where $\boldsymbol{K}_0^{P}$ and $\boldsymbol{F}_0^{P}$ are the piezoelectric geometric matrix and force vector under unit piezoelectric potentials. The out-of-balance vector $\boldsymbol{q}(\boldsymbol{u}_s, \lambda_P)$ is linearized with respect to $\boldsymbol{u}_s$ and λ_P at the $(i+1)$th iteration step using the truncated Taylor series expansion to formulate an incremental iterative equation:

$$\boldsymbol{q}^{i+1} \cong \boldsymbol{q}^i\left(\boldsymbol{u}_s^i, \lambda_P^i\right) + \frac{\partial\boldsymbol{q}^i}{\partial\boldsymbol{u}_s}\delta\boldsymbol{u}_s^{i+1} + \frac{\partial\boldsymbol{q}^i}{\partial\lambda_P}\delta\lambda_P^{i+1} = \boldsymbol{0} \tag{15}$$

Consequently, the iterative change of displacements $(\delta\boldsymbol{u}_s^{i+1})$ at the $(i+1)$th iteration step can be arranged as

$$\delta\boldsymbol{u}_s^{i+1} = \frac{\partial\boldsymbol{q}^i}{\partial\boldsymbol{u}_s}^{-1}\left(-\boldsymbol{q}^i\left(\boldsymbol{u}_s^i, \lambda_P^i\right) - \delta\lambda_P^{i+1}\frac{\partial\boldsymbol{q}^i}{\partial\lambda_P}\right) = \delta\bar{\boldsymbol{u}}_s^i + \delta\lambda_P^{i+1}\delta\boldsymbol{u}_{sT}^i \tag{16}$$

where

$$\frac{\partial\boldsymbol{q}^i}{\partial\boldsymbol{u}_s} = \boldsymbol{K0} - \lambda_P^i\boldsymbol{K}_0^{P} - \boldsymbol{K}^{\Delta T} + \boldsymbol{KN1}\left(\boldsymbol{u}_s^i\right) + \boldsymbol{KN2}\left(\boldsymbol{u}_s^i\right) \tag{17}$$

$$\frac{\partial\boldsymbol{q}^i}{\partial\lambda_P} = -\boldsymbol{K}_0^{P}\boldsymbol{u}_s^i - \boldsymbol{F}_0^{P} \tag{18}$$

where the relationships between incremental quantity Δ and iterative quantity δ are

$$\lambda_P^{i+1} = \lambda_P^i + \delta\lambda_P^{i+1}, \qquad \Delta\lambda_P^{i+1} = \Delta\lambda_P^i + \delta\lambda_P^{i+1} \tag{19a}$$

$$\boldsymbol{u}_s^{i+1} = \boldsymbol{u}_s^i + \delta\boldsymbol{u}_s^{i+1}, \qquad \Delta\boldsymbol{u}_s^{i+1} = \Delta\boldsymbol{u}_s^i + \delta\boldsymbol{u}_s^{i+1} \tag{19b}$$

To solve unknown values $\delta\boldsymbol{u}_s^{i+1}$ and $\delta\lambda_P^{i+1}$, a scalar additional equation, namely, the cylindrical arc-length equation, is applied in the following form:

$$\Delta\boldsymbol{u}_s^{i+1\,T}\Delta\boldsymbol{u}_s^{i+1} = \Delta\boldsymbol{u}_s^{i\,T}\Delta\boldsymbol{u}_s^i = \Delta l^2 \tag{20}$$

Substitution of Eqs. (16) and (19) into Eq. (20) yields the following quadratic equation for the iterative load level $(\delta\lambda_P^{i+1})$:

$$a_1\delta\lambda_P^{i+1\,2} + a_2\delta\lambda_P^{i+1} + a_3 = 0 \tag{21}$$

where

$$a_1 = \delta\boldsymbol{u}_{sT}^{i\,T}\delta\boldsymbol{u}_{sT}^i$$

$$a_2 = 2\delta\boldsymbol{u}_{sT}^{i\,T}\left(\Delta\boldsymbol{u}_s^i + \delta\bar{\boldsymbol{u}}_s^i\right)$$

$$a_3 = \left(\Delta\boldsymbol{u}_s^i + \delta\bar{\boldsymbol{u}}_s^i\right)^T\left(\Delta\boldsymbol{u}_s^i + \delta\bar{\boldsymbol{u}}_s^i\right) - \Delta l^2 \tag{22}$$

where $\delta\lambda_P^{i+1}$, which gives an acute angle between $\Delta\boldsymbol{u}_s^i$ and $\Delta\boldsymbol{u}_s^{i+1}$, is chosen to avoid doubling back on the load-displacement path. Arc length Δl with a given initial incremental load level $\Delta\lambda_P^0$ is determined as

$$\Delta l = \Delta\lambda_P^0\sqrt{\delta\boldsymbol{u}_{sT}^{1\,T}\delta\boldsymbol{u}_{sT}^1} \tag{23}$$

The constant arc length Δl is used at all iteration steps. The convergence criterion of displacement with $\varepsilon_u = 1.0 \times 10^{-5}$ is given as

$$\|\delta\boldsymbol{u}\| / \|\Delta\boldsymbol{u}\| \le \varepsilon_u \tag{24}$$

The estimation of an initial load level in the new load step is very important. An incorrect initial load level induces oscillation and reversion of the load-displacement path. For the initial load factor in the new load step, $\delta\lambda_{P,\text{new step}}^1$ satisfying the following condition is chosen:

$$\Delta u_{s,\text{old step}}^{\text{last}\;T}\delta u_{s,\text{new step}}^1 > 0 \tag{25}$$

Vibration Analysis of Thermopiezoelastic Systems

After obtaining the converged thermopiezoelastic large deflection, the vibration analysis of thermopiezoelectrically deformed plates can be performed by solving Eq. (9) as an eigenvalue problem under the assumption of small harmonic oscillation:

$$\left[\boldsymbol{K0} - \boldsymbol{K}^{\Delta T} - \lambda_P\boldsymbol{K}_0^{P} + \boldsymbol{KN1}(\boldsymbol{u}_s) + \boldsymbol{KN2}(\boldsymbol{u}_s) - \omega^2\boldsymbol{M}\right]\{\Phi\} = \boldsymbol{0} \tag{26}$$

We applied a skyline storage scheme to the construction of system matrix and used a subspace iteration method[28] assuming positive definite stiffness in the eigenvalue analysis. Thus we skipped the vibration analysis in the range of the non-positive definite system, resulting in a negative eigenvalue for the thermopiezoelastic plate, which often occurs in the snap-through behaviors.

Results and Discussion

Verification of Finite Element Code

To validate the present layerwise finite element programs, we solved the thermal postbuckling, linear thermopiezoelastic

deformation, and free vibration problems and compared the obtained results with those in the open literature. First, we analyzed the thermal postbuckling problems of the $[+45/-45/0/90]_s$ and $[(+15/-15)_2]_s$ laminated square plates solved by Averil and Reddy[29] and by Lee and Lee,[30] respectively. The thickness of each layer is 0.125 mm, and the planar axial length of the square plate is 150 mm. The material used here is the typical graphite–epoxy as in Refs. 29 and 30. Simply supported boundary conditions in the present layerwise model are

$$W = U^m = 0 \qquad \text{at } x = 0, a \tag{27a}$$

$$W = V^m = 0 \qquad \text{at } y = 0, b \tag{27b}$$

where m is an in-plane interface at the midplane of base composite plate. The normalized maximum deflection of the plate according to the temperature increase is presented in Fig. 2 and compared with previous results. Figure 2 indicates that present results are in good agreement with those of Refs. 29 and 30, although showing slightly lower buckling temperatures and larger deflection due to the difference of displacement fields.

Second, the piezoelectric transverse deflection of a three layer active beam has been analyzed and compared with the results by Saravanos and Heyliger.[7] When the electric potential 12.49 kV is applied between the upper and lower electrodes of the PZT-4 layer, the transverse deflection of the active beam is presented in Fig. 3. Excellent agreement can be shown between the present results and results by Saravanos and Heyliger.[7]

The third problem is the active thermal distortion management of thermopiezoelastic plates, previously examined by Ha et al.[14] The

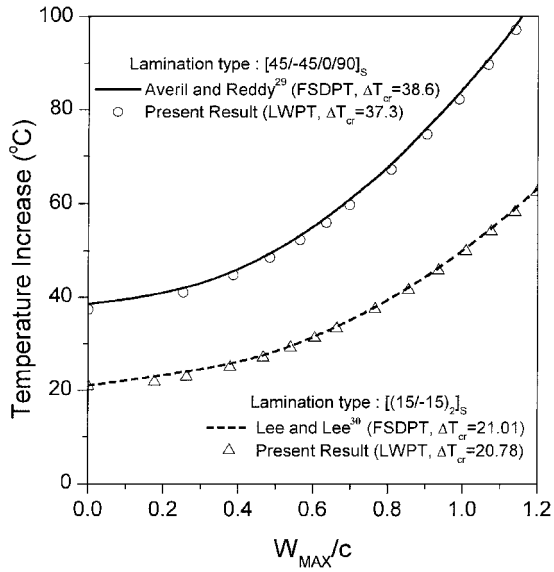

Fig. 2 Thermal postbuckling of simply supported square [0/± 45/90]$_s$ and [(+15/− 15)2]$_s$ laminated plates with $a/c = 150$.

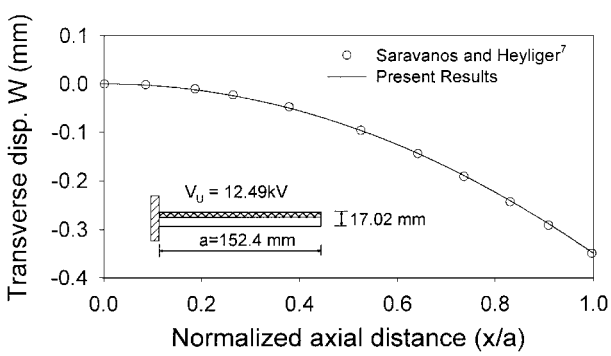

Fig. 3 Static transverse deflection for the active peizolaminated beam subject to piezoelectric load.

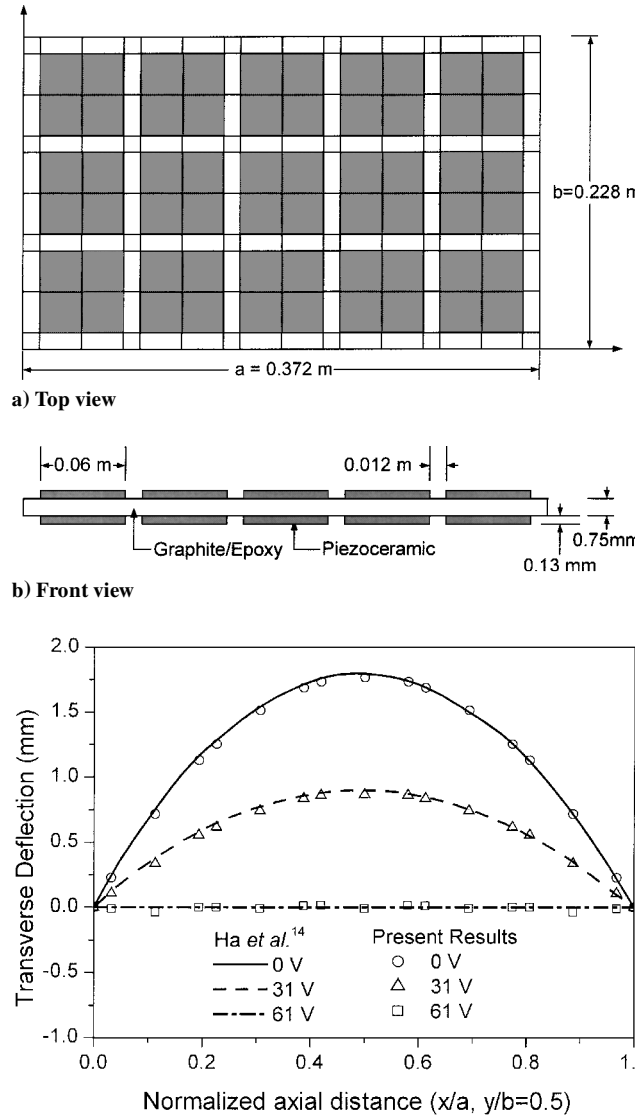

Fig. 4 Geometry of piezolaminated plate and comparison of linear thermopiezoelastic behavior.

objective of this work is to suppress the thermal distortion induced by a thermal gradient by applying electric fields to both top and bottom piezoceramic patches. Geometry and finite element meshes are shown in Figs. 4a and 4b, and material properties are listed in Table 1. The plate is simply supported along the two edges parallel to the y axis and is free on the two edges parallel to the x axis. Initially, the plate is exposed to an elevated environment with temperature increase of 27.777°C (50°F) on the top surface and with temperature drop of 27.777°C on the bottom surface from the reference temperature. It is assumed that the temperature distribution is quasi steady and linear in the thickness direction. Figure 4c shows the reduction in the transverse deflection achieved by applying an active voltage of 61 V and good agreement with results by Ha et al.[14]

Last, we compared the natural frequencies of simply supported [0/90/0] laminated plates with the previous results obtained by exact three-dimensional elasticity,[31] full layerwise theory,[32] and equivalent single-layer theories.[31] Each ply is assumed to be orthotropic with nine independent material properties: $E_1 = 25.1 \times 10^6$ psi, $E_2 = 4.8 \times 10^6$ psi, and $E_3 = 0.75 \times 10^6$ psi; $G_{12} = 1.36 \times 10^6$ psi, $G_{13} = 1.2 \times 10^6$ psi, and $G_{23} = 0.47 \times 10^6$ psi; and $\nu_{12} = 0.036$, $\nu_{13} = 0.25$, and $\nu_{23} = 0.171$. The 4×4 meshes with nine-node elements are used. The thickness of a lamina is 0.125 mm, and total thickness ratio of the laminate is $a/c = 10$. It is considered a very thick plate. Table 2 compares present partial layerwise finite

Table 1 Material properties of the graphite–epoxy and PZT-5A layers

Property	Graphite–epoxy	PZT-5A
E_1, GPa	150	63
E_2, GPa	9.0	63
G_{12}, GPa	7.1	24.2
G_{23}, GPa	2.5	24.2
ν_{12}	0.3	0.3
α_1, 10^{-6}/°C	1.1	0.9
α_2, 10^{-6}/°C	25.2	0.9
e_{31}, 10^{-12} m/V	0	254
e_{32}, 10^{-12} m/V	0	254
ρ, kg/m^3	1600	7600
c_{lamina}, mm	0.125	$c_{SF}=0.1000$ $c_{SP}=0.2086$ $c_{EF}=0.2000$ $c_{EP}=0.4173$
Reference temperature, °C	20	20

Table 2 Comparison of nondimensional natural frequencies for simply supported [0/90/0] laminated square plates: $\varpi=\omega c\sqrt{(\rho/E_2)}$, $a/c=10$

Theory	ϖ_1	ϖ_2	ϖ_3	ϖ_4
Exact solution[31] (three-dimensional elasticity)	0.06715	0.12811	0.17217	0.20798
LWPT[a] (Carrera,[32] LDL[b])	0.06758	——	——	0.21100
Present results (partial LWPT[a])	0.06629	0.12862	0.17364	0.20913
TSDPT[31]	0.06839	0.13010	0.17921	0.21526
FSDPT[31]	0.06931	0.12886	0.18674	0.22055
CLPT[31]	0.07769	0.15185	0.26599	0.31077

[a]Layerwise laminated plate theory.
[b]Layerwise displacement theory with linear interpolation functions.

element solutions with the results by exact three-dimensional elasticity, full layerwise theory, third-order shear deformation plate theory (TSDPT), first-order shear deformation plate theory (FSDPT), and classical laminated plate theory (CLPT) for the lower four nondimensional natural frequencies. The present partial layerwise model gives good solutions comparable with the results by exact three-dimensional elasticity[31] and full layerwise theory.[32]

Model of Thermopiezoelastic Plates

Four kinds of piezolaminated plates are taken as analysis models as shown in Fig. 5. It is assumed that piezoelectric layers are perfectly bonded on the surface of base composite laminate for all models: symmetrically and fully covered piezolaminated plate (SF), symmetrically and partially covered piezolaminated plate (SP), eccentrically and fully covered piezolaminated plate (EF), and eccentrically and partially covered piezolaminated plate (EP).

The 13×13 meshes with nine-node finite elements are used as shown in Fig. 5. The material properties and thickness of a lamina and piezoceramics are given in Table 1. Note that the thickness of piezoelectric actuators is different so that all plates have the same volume of total piezoelectric actuators. The dimension of the composite base plate is $a=b=120$ mm and $c_{\text{base}}=1$ mm. The base composite structure is a $[0/+45/-45/90]_s$ square graphite–epoxy laminated plate with all simply supported edges. Simply supported boundary conditions in the present analysis are

$$W=U^m=0 \qquad \text{at } x=0,a \tag{28a}$$

$$W=V^m=0 \qquad \text{at } y=0,b \tag{28b}$$

where m is an in-plane interface at the midplane of base composite plate.

According to the patterns of applied electric potential, different actuation modes can be obtained, as shown in Fig. 6. Symmetrically piezolaminated plates have four types of actuation modes; two of which are in-phase actuation modes, and the rest are out-of-phase actuation modes resulting in bending moments. Eccentrically piezolaminated plates have only two actuation modes. In this case, the in-plane and bending modes are always coupled.

Table 3 Euler buckling temperature and natural frequencies of piezolaminated composite plate

Structural model	Euler buckling temperature, °C	Natural frequency, Hz				
		f_1	f_2	f_3	f_4	f_5
SF	50.241	374.21	854.26	1065.8	1517.7	1725.5
SP	44.867	340.89	762.16	1009.0	1398.1	1680.4
EF	52.632	383.02	854.96	1066.6	1522.0	1728.9
EP	46.193	346.19	766.61	1016.0	1410.8	1701.1

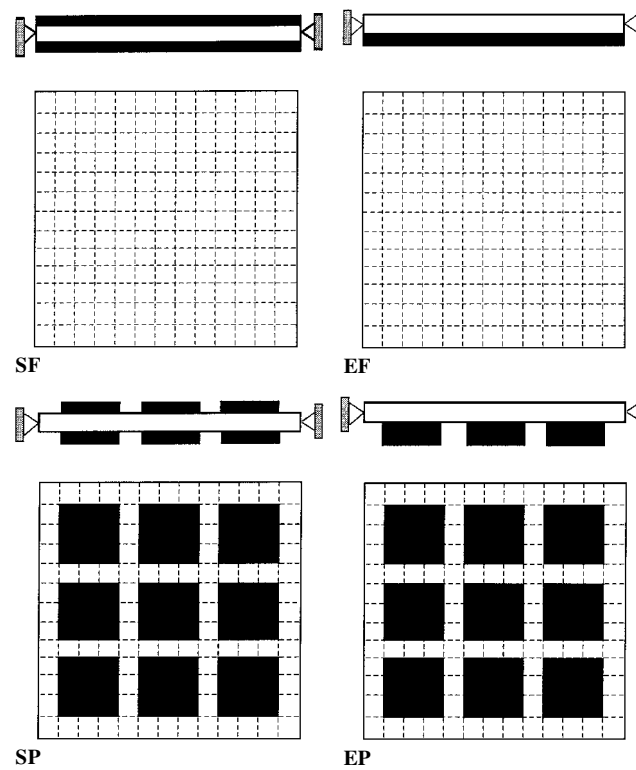

Fig. 5 Structural models of pizolaminated plates with surface bonded piezoactuators.

Thermal Buckling and Free Vibration of Piezolaminated Plate

The results of thermal buckling and free vibration analyses for four different structural models are presented in Table 3. It is well known that eccentric piezolaminated plates subject to in-plane compressive loads show a monotonous increase in the load-displacement diagram unlike symmetric piezolaminated plates with bifurcation buckling at a critical temperature. In eccentric piezolaminated plates, we used an Euler buckling temperature obtained from Eq. (10) to use as a reference temperature that is a denominator in the nondimensional temperature parameter. Fully covered models have higher buckling temperatures than partially covered models. In addition, vibration frequencies of fully covered models are generally higher than those of partially covered models. Among four models, the EF model has the highest natural frequencies due to the eccentricity of piezoactuators.

Thermal Postbuckling and Vibration of Piezolaminated Plate

Figure 7a shows thermal postbuckling behaviors of piezolaminated flat panels. Symmetric structural models have bifurcation buckling characteristics, and eccentric models exhibit negative deflections without bifurcation buckling under uniform temperature distribution. Buckling temperatures from the thermal postbuckling analysis are slightly higher than the results by linear Euler buckling

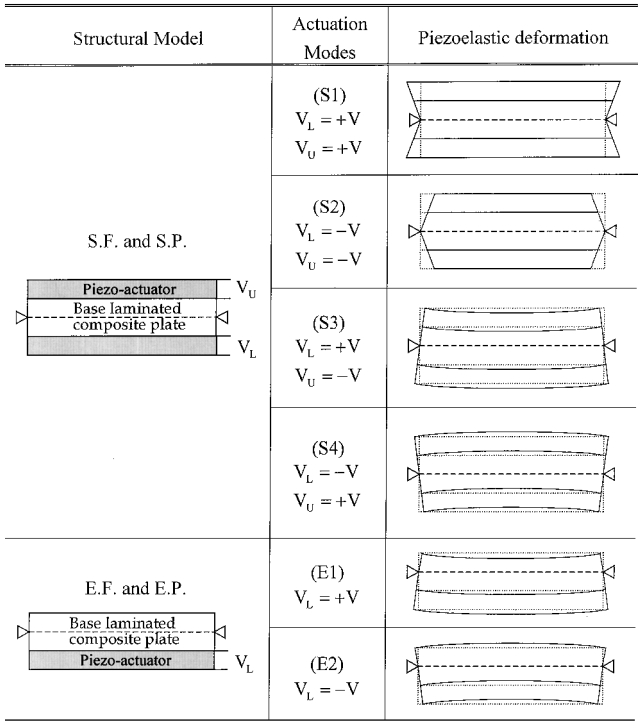

Fig. 6 Piezoelastic deformation according to various actuation modes.

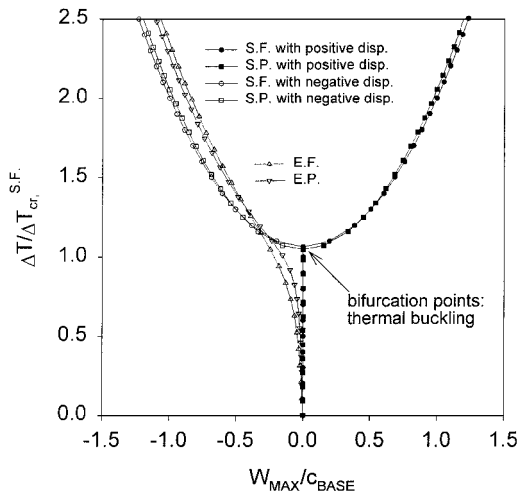

a) Thermal postbuckling

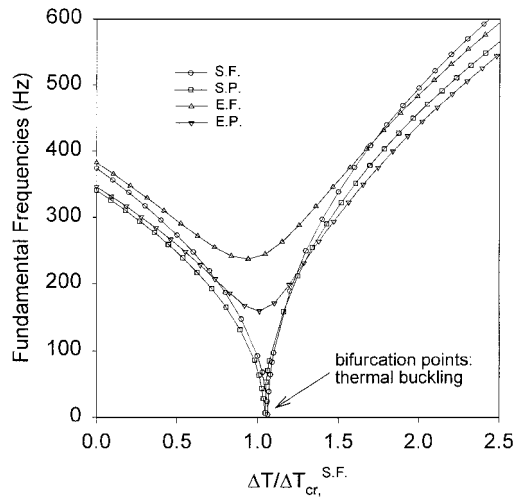

b) Vibration characteristics

Fig. 7 Thermal postbuckling and vibration characteristics of piezolaminated plates.

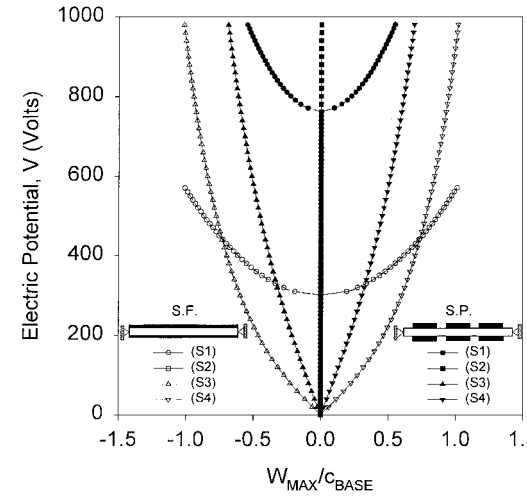

a) Piezoelastic deflection

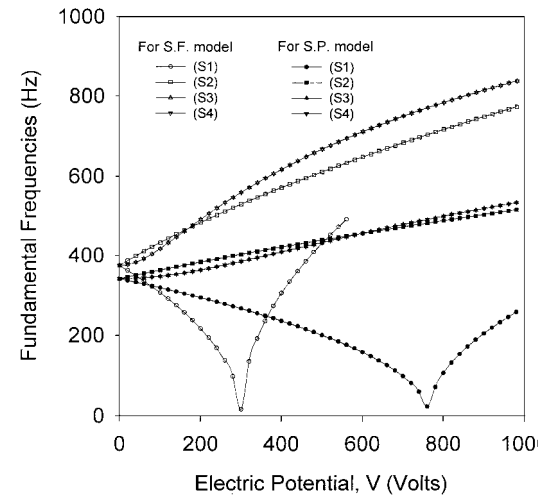

b) History of fundamental frequency

Fig. 8 Piezoelastic postbuckling and vibration characteristics of symmetrically piezolaminated plates.

analysis. Vibration characteristics of piezolaminated plates subject to thermal loads are presented in Fig. 7b. At the bifurcation buckling points, fundamental frequencies corresponding to buckling mode have almost zero values for symmetric models. As the postbuckled deflection increases above the buckling point, natural frequencies increase due to geometric nonlinearity induced by thermally large deflection. Frequencies of eccentric structural models without bifurcation points do not show steep drops unlike symmetric models.

Piezoelastic Deformation and Vibration Analysis

Piezoelastic deformation and vibration analyses for various actuation modes are performed. Piezoleastic behaviors of symmetric models are shown in Fig. 8. When the electric potential is applied according to an S1 actuation, in which the piezoelectric actuators generate induced tensile strain and in the end give compressive loads to the base composite plate with immovable edges as shown in Fig. 6, both SF and SP models show piezoelastic bifurcation buckling and postbuckling behaviors in Fig. 8a. It can be found that SP model has higher piezoelectric buckling potential. An S2 actuation mode does not generate transverse deflections up to high voltage, as expected. In S3 and S4 actuation modes, piezoelectric actuators induce bending moments by out-of-phase actuation, so that both models have transverse deflections even with low electric potential. Frequency variations according to the applied electric potential are presented in Fig. 8b. When the electric potential is applied according to S1 actuation mode, fundamental frequencies of both SF and SP models approach to zero at the piezoelectric bifurcation buckling

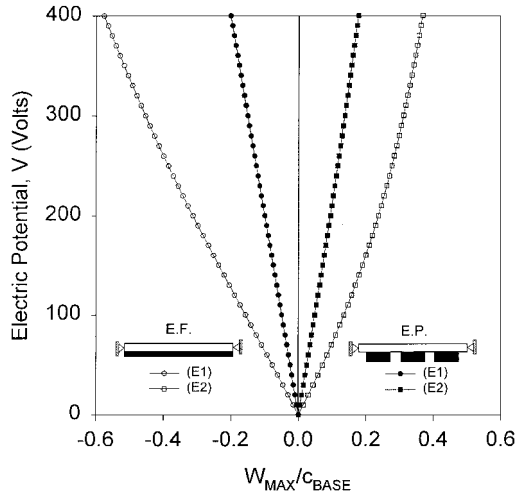

a) Piezoelastic deflection

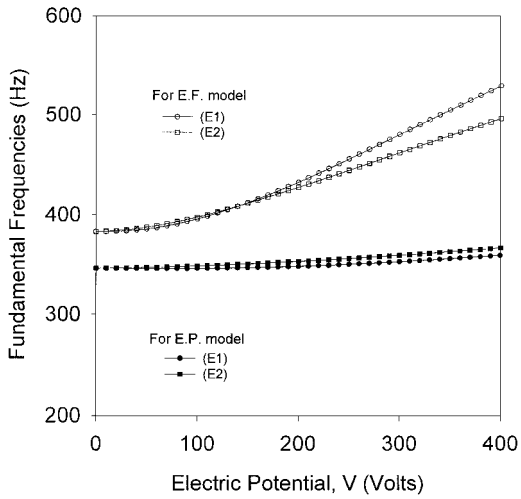

b) Vibration characteristics

Fig. 9 Piezoelastic nonlinear deflections and vibration characteristics of eccentrically piezolaminated plates.

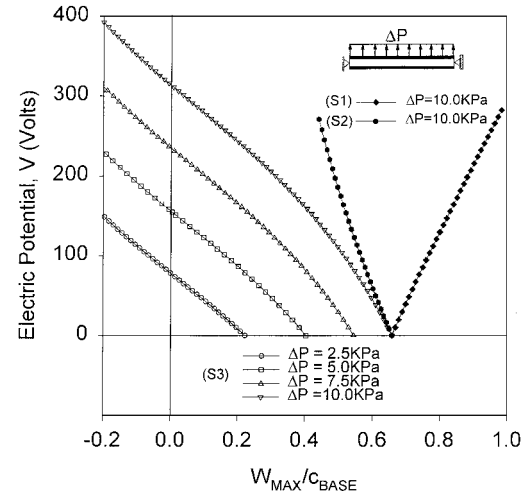

a) Suppressed deflection

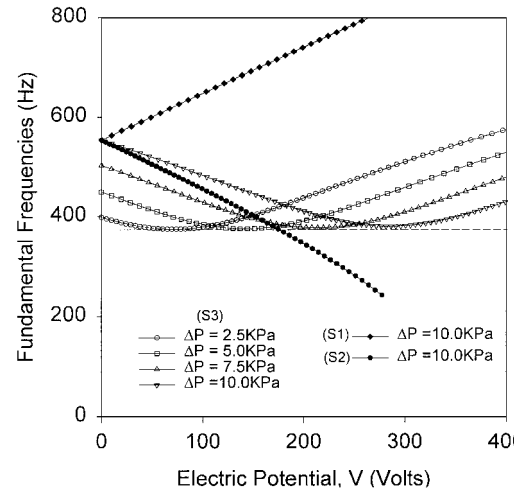

b) History of fundamental frequencies

Fig. 10 Suppressed deflection and frequency history of SF model under transverse surface pressure.

points. The fundamental frequencies of the plates monotonously increase when negative electric potentials are applied to both upper and lower piezoelectric layers, that is, in S2 actuation mode, due to induced tensile stresses. The frequency histories of the plates in S3 and S4 actuation modes are the same; fundamental frequencies increase monotonically as the applied electric potential increases.

The piezoelastic behaviors of eccentric piezolaminated plates EF and EP are investigated. Figure 9a shows the piezoelectrically induced transverse deflections. Because of the eccentricity of piezoactuators, E1 and E2 actuation modes do not show symmetric piezoelastic deformation curves in Fig. 9a. It can be found that a fully covered model has larger deflections than a partially covered model. Also, E1 actuation, in which piezoelectric actuators generate tensile strain, yields larger transverse deflections than E2 actuation. Fundamental frequencies of both models EF and EP monotonically increase as the applied electric potential increases, as shown in Fig. 9b. However, it can be found that the increase of natural frequency for the EF model is more noticeable. This is because the EF model has larger piezoelectrically induced deflections, as can be seen in Fig. 9a, so that the geometrically stiffening effect is more dominant.

Piezoelectric Suppression of Large Deflection due to Surface Pressure

Piezoelectric suppression of large deflections due to the transverse surface pressure is investigated and presented in Fig. 10 for the SF model. Three actuation modes, namely, S1, S2, and S3, are tested for the reduction of large deflections caused by a transverse loading. Figure 10a shows that S3 actuation is more efficient than S1 and S2 actuations under a large pressure differential, $\Delta P = 10.0$ kPa. Therefore, the proper out-of-phase actuation can be used to reduce effectively transverse deflections due to the surface pressure. For various pressure loads, we can find optimal piezoelectric potential for the suppression of deflections without unstable behaviors. Vibration characteristics of the plate under the surface pressure are shown for various electric potentials in Fig. 10b. When the reduced transverse deflection by a piezoelectric suppression reaches almost zero, fundamental frequencies approach natural frequencies of the plate without surface pressure. The present results show that the piezoelectric out-of-phase actuation, that is, S3 actuation, can successfully suppress the large deflection due to a transverse surface pressure.

Thermopiezoelastic Buckling, Postbuckling, and Snapping Phenomena

First, thermopiezoelastic buckling analysis of symmetric structural models SF and SP is performed. The enhancement of thermal buckling temperature using piezoelectric actuation by the piezoelectrically induced in-phase actuation is shown in Fig. 11. A fully covered piezolaminated plate is more effective to enhance the thermal buckling temperature than a partially covered plate. The results show that thermal buckling temperature of the SF model under $V = -300$ V in the S2 actuation mode is twice the buckling temperature without piezoelectric actuation.

Next, the nonlinear thermopiezoelastic behavior of SF in the S3 actuation mode is investigated. Figure 12a shows the transverse deflection of the centerpoint of the plate under five temperature

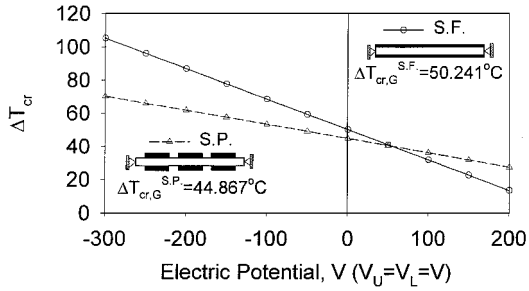

Fig. 11 Enhancement of thermal buckling temperature for symmetric structural models using in-phase piezoelectric actuation.

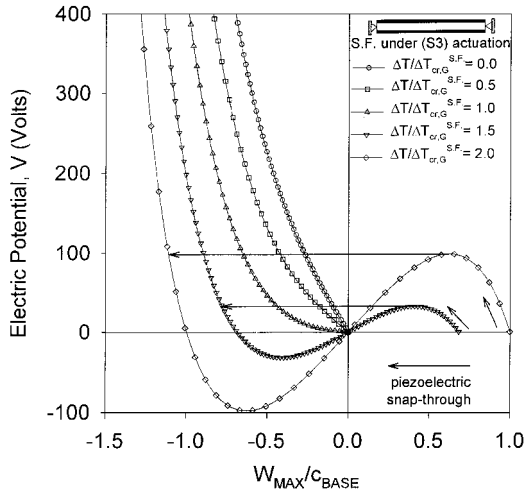

a) Thermopiezoelastic snap-through

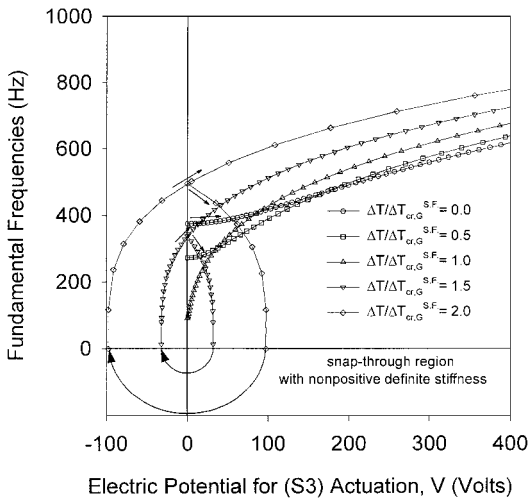

b) Vibration characteristics

Fig. 12 Thermopiezoelastic snap-through phenomena and vibration characteristics of SF model with S3 actuation under thermal pre- and postbuckling states.

states, $\Delta T/\Delta T_{cr,G}^{SF} = 0.0$, 0.5, 1.0, 1.5, and 2.0, when the piezoelectric bending moment due to S3 actuation is applied. In other words, thermopiezoelastic deflection under a thermal prebuckling state at $\Delta T/\Delta T_{cr,G}^{SF} = 0.0$, 0.5, and 1.0 has negative deflection caused by the moment direction of an S3 actuation. Under thermal postbuckling states $\Delta T/\Delta T_{cr,G}^{SF} = 1.5$ and 2.0, the deflections are reduced as the electric voltages increase. However, at certain electric potentials, another kind of instability is found like snap-through. We refer to these phenomena as thermopiezoelastic snap-through. Generally, snap-through phenomena occur in the buckling process of curved panels and shells under compressive and transverse loads. To analyze the instability of thermopiezoelastic snapping phenomena, the cylindrical arc-length method is adopted. Figure 12a shows that

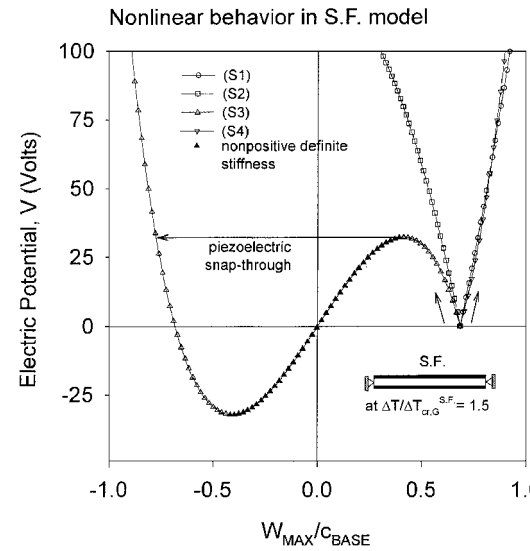

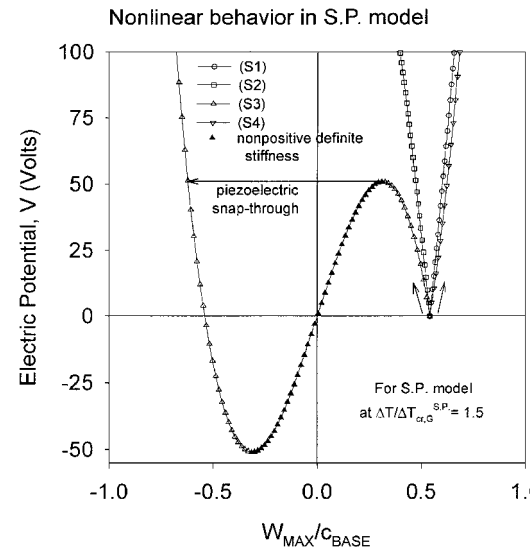

Fig. 13 Nonlinear thermopiezoelastic behaviors of SF and SP models by various actuation modes under thermally postbuckled state.

voltage-displacement paths always pass the origin and have antisymmetric characteristics on the $x-y$ axes. Vibration characteristics of thermopiezoelastic plates are shown in Fig. 12b. In the cases of prebuckling, $\Delta T/\Delta T_{cr,G}^{SF} = 0.0$, 0.5, and 1.0, fundamental frequencies increase as the electric voltage increases. However, in the cases of postbuckling, $\Delta T/\Delta T_{cr,G}^{SF} = 1.5$, and 2.0, fundamental frequency dramatically decreases until the snap-through electric voltage and has negative values over that point. As the voltage-displacement path goes over, the stiffness matrix again gives positive eigenvalues. Symmetric characteristics of vibration history on the y axis are shown before and after snap-through.

The effectiveness of actuation modes for the suppression of a thermally postbuckled plate is investigated for the SF and SP model with $\Delta T/\Delta T_{cr,G} = 1.5$. Figure 13 shows that S1 and S4 actuations increase thermally buckled deflections. Both S2 and S3 actuations can reduce the thermally buckled deflections; however, S3 actuation mode yields thermopiezoelastic snapping behaviors. Through a snap-through, a piezoelectric actuation in the S3 mode can abruptly shift the static deformation. Therefore, the S3 actuation mode, which was efficiently used in the suppression of large deflection due to a transverse surface pressure, cannot perfectly suppress the thermally buckled deflection because of the thermopiezoelastic snapping.

The last example is about the nonlinear thermopiezoelastic behaviors of eccentric piezolaminated plates. Eccentric structural models have negative transverse deflections under uniform thermal loading. Thus, E2 actuation mode is used to suppress thermoelastic deflections under $\Delta T/\Delta T_{cr,G} = 0.5$, 1.0, and 1.5. Figure 14 shows that

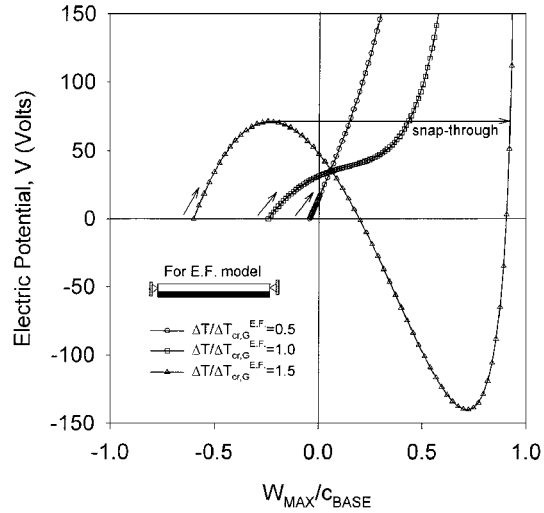

EF model

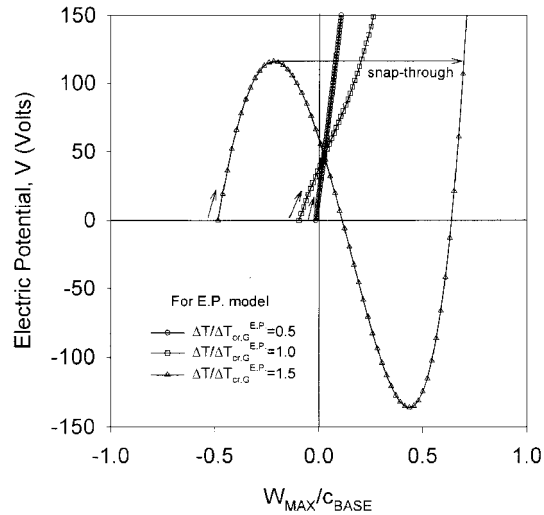

EP model

Fig. 14 Nonlinear thermopiezoelastic behaviors of EF and EP models with E2 actuation for various temperatures.

the piezoelastic suppression of thermally buckled deflections cannot be perfectly achieved above critical temperatures because of a snap-through. However, thermoelastic deformation below a critical temperature can be efficiently suppressed. Unlike a symmetric structural model, the snapping behaviors do not have symmetric characteristics about the origin.

Consequently, great care should be taken of the placement and size of piezoelectric layers and optimal control voltages with suitable actuation modes in the active suppression of postbuckled shape to avoid possible snap-through phenomena, resulting in jump to another equilibrium state.

Conclusions

The nonlinear thermopiezoelastic behavior of piezolaminated plates is investigated using layerwise nonlinear finite elements. The cylindrical arc-length scheme and Newton–Raphson method are applied to take into account thermopiezoelastic snapping phenomena. Numerical results are provided for symmetric and eccentric structural models with various actuation modes, and the following conclusions can be drawn from the present results.

1) Piezoelectrically induced in-plane loads by an S2 actuation mode can successfully increase thermal buckling temperatures for the symmetric structural models.

2) For symmetric structural models, postbuckled deflections due to compressive in-plane thermal stresses may not be reduced in an S3 actuation mode because of thermopiezoelastic snap-through phenomena, although a large deflection due to a transverse surface pressure can be efficiently suppressed by an S3 actuation mode.

3) For eccentric structural models without bifurcation buckling phenomena, thermoelastic deformation below a critical temperature distribution can be efficiently suppressed. However, the piezoelectric suppression of large thermal deflections cannot be perfectly achieved above the critical temperature because of the thermopiezoelastic snap-through.

4) The vibration characteristics of piezolaminated plates subject to compressive thermal loads have close relationships with buckling and postbuckling behaviors. When the applied piezoelectric loads reduce the thermal deflection, the frequencies can be dramatically decreased. Also, the snap-through path in the electric potential-deflection relation shows the nonpositive definite stiffness, resulting in negative eigenvalues.

The present results show that an excessive piezoelectric actuation for the suppression of buckled deflection may cause snapping phenomena, resulting in a jump to another equilibrium state. Therefore, great care should be taken of the placement and size of piezoelectric layers, actuation modes, and possible snap-through phenomena, for the active suppression of postbuckled shape.

References

[1]Crawley, E. F., and de Luis, J., "Use of Piezoelectric Actuators as Elements of Intelligent Structures," *AIAA Journal*, Vol. 25, No. 10, 1987, pp. 1373–1385.

[2]Wang, B. T., and Rogers, C. A., "Laminate Plate Theory for Spatially Distributed Induced Strain Actuators," *Journal of Composite Materials*, Vol. 25, No. 4, 1991, pp. 433–452.

[3]Lee, C. K., "Theory of Laminated Piezoelectric Plates for the Design of Distributed Sensors/Actuators. Part I: Governing Equations and Reciprocal Relationships," *Journal of the Acoustical Society of America*, Vol. 87, No. 3, 1990, pp. 1144–1158.

[4]Tzou, H. S., and Tseng, C. I., "Distributed Piezoelectric Sensor/Actuator Design for Dynamic Measurement/Control of Distributed Parameter Systems: A Piezoelectric Finite Element Approach," *Journal of Sound and Vibration*, Vol. 138, No. 1, 1990, pp. 17–34.

[5]Han, J. H., and Lee, I., "Active Damping Enhancement of Composite Plates with Electrode Designed Piezoelectric Materials," *Journal of Intelligent Material Systems and Structures*, Vol. 8, No. 12, 1997, pp. 249–259.

[6]Robbins, D. H., and Reddy, J. N., "Analysis of Piezoelectrically Actuated Beams Using a Layerwise Displacement Theory," *Computers and Structures*, Vol. 41, No. 2, 1991, pp. 265–279.

[7]Saravanos, D. A., and Heyliger, P. R., "Coupled Layerwise Analysis of Composite Beams with Embedded Piezoelectric Sensors and Actuators," *Journal of Intelligent Material Systems and Structures*, Vol. 6, No. 3, 1995, pp. 350–363.

[8]Heyliger, P. R., Ramirez, G., and Saravanos, D., "Coupled Discrete-Layer Finite Elements for Laminated Piezoelectric Plates," *Communications in Numerical Methods in Engineering*, Vol. 10, No. 12, 1994, pp. 971–981.

[9]Han, J. H., and Lee, I., "Analysis of Composite Plates with Piezoelectric Actuators for Vibration Control Using Layerwise Displacement Theory," *Composites: Part B, Engineering*, Vol. 29, No. 5, 1998, pp. 621–632.

[10]Tzou, H. S., and Ye, R., "Analysis of Piezoelastic Structures with Laminated Piezoelectric Triangular Shell Elements," *AIAA Journal*, Vol. 34, No. 1, 1996, pp. 110–115.

[11]Meressi, S., and Paden, B., "Buckling Control of a Flexible Beam Using Piezoelectric Actuators," *Journal of Guidance, Control, and Dynamics*, Vol. 16, No. 5, 1993, pp. 977–980.

[12]Thomson, S. P., and Loughlan, J., "The Active Buckling Control of Some Composite Column Strips Using Piezoceramic Actuators," *Composite Structures*, Vol. 32, Nos. 1–4, 1995, pp. 59–67.

[13]Faria, A. R., and Almeida, S. F. M., "Enhancement of Pre-Buckling Behavior of Composite Beams with Geometric Imperfections Using Piezoelectric Actuators," *Composites: Part B, Engineering*, Vol. 30, No. 1, 1999, pp. 43–50.

[14]Ha, S. K., Keilers, C., and Chang, F. K., "Finite Element Analysis of Composite Structures Containing Distributed Piezoceramic Sensors and Actuators," *AIAA Journal*, Vol. 30, No. 3, 1992, pp. 772–780.

[15]Tzou, H. S., and Ye, R., "Piezothermoelasticity and Precision Control of Piezoelectric Systems: Theory and Finite Element Analysis," *Journal of Vibration and Acoustics*, Vol. 116, No. 4, 1994, pp. 489–495.

[16]Lee, H. J., and Saravanos, D. A., "Generalized Finite Element Formulation for Smart Multilayered Thermal Piezoelectric Composite Plates," *International Journal of Solids and Structures*, Vol. 34, No. 26, 1997, pp. 3355–3371.

[17]Smittakorn, W., and Heyliger, P. R., "A Discrete-Layer Model of Laminated Hygrothermopiezoelectric Plates," *Mechanics of Composite Materials and Structures*, Vol. 7, No. 1, 2000, pp. 79–104.

[18]Barbero, E. J., and Reddy, J. N., "Nonlinear Analysis of Composite Laminates Using a Generalized Laminated Plate Theory," *AIAA Journal*, Vol. 28, No. 11, 1994, pp. 1987–1994.

[19]Pai, P. F., Nayfeh, A. H., Oh, K., and Mook, D. T., "A Refined Nonlinear Model of Piezoelectric Plates," *International Journal of Solids and Structures*, Vol. 30, No. 12, 1993, pp. 1603–1630.

[20]Tzou, H. S., and Zhou, Y. H., "Nonlinear Piezothermoelasticity and Multi-Field Actuations, Part 2: Control of Nonlinear Deflection, Buckling and Dynamics," *Journal of Vibration and Acoustics*, Vol. 119, No. 3, 1997, pp. 382–389.

[21]Bao, Y., Tzou, H. S., and Venkayya, V. B., "Analysis of Nonlinear Piezothermoelastic Laminated Beams with Electric and Temperature Effects," *Journal of Sound and Vibration*, Vol. 209, No. 3, 1998, pp. 505–518.

[22]Oh, I. K., Han, J. H., and Lee, I., "Postbuckling and Vibration Characteristics of Piezolaminated Composite Plate Subject to Thermopiezoelectric Loads," *Journal of Sound and Vibration*, Vol. 233, No. 1, 2000, pp. 19–40.

[23]Crisfield, M. A., *Non-Linear Finite Element Analysis of Solids and Structures*, Vol. 1, Wiley, New York, 1997, pp. 252–333.

[24]Librescu, L., Lin, W., Nemeth, M. P., and Starnes, J. H., Jr., "Vibration of Geometrically Imperfect Panels Subjected to Thermal and Mechanical Loads," *Journal of Spacecraft and Rockets*, Vol. 33, No. 2, 1996, pp. 285–291.

[25]Reddy, J. N., *Mechanics of Laminated Composite Plates: Theory and Analysis*, CRC Press, New York, 1997, pp. 651–722.

[26]Tiersten, H. F., *Linear Piezoelectric Plate Vibrations*, Plenum, New York, 1969, pp. 33–39.

[27]Benjeddou, A., "Advances in Piezoelectric Finite Element Modeling of Adaptive Structural Elements: A Survey," *Computers and Structures*, Vol. 76, No. 1–3, 2000, pp. 347–363.

[28]Bathe, K. J., *Finite Element Procedure*, Prentice–Hall, Upper Saddle River, NJ, 1996, pp. 954–978.

[29]Averil, R. C., and Reddy, J. N., "Thermomechanical Postbuckling Analysis of Laminated Composite Shells," *Proceedings of AIAA/ASME/ASCE/AHS/ASC 34th Structures, Dynamics, and Materials Conference*, AIAA, Washington, DC, 1993, pp. 351–360.

[30]Lee, D. M., and Lee, I., "Vibration Behaviors of Thermally Postbuckled Anisotropic Plates Using First-Order Shear Deformable Plate Theory," *Computers and Structures*, Vol. 63, No. 3, 1997, pp. 371–378.

[31]Nosier, A., Kapania, R. K., and Reddy, J. N., "Free Vibration Analysis of Laminated Plates Using a Layerwise Theory," *AIAA Journal*, Vol. 31, No. 12, 1993, pp. 2335–2346.

[32]Carrera, E., "An Assessment of Mixed and Classical Theory on Global and Local Response of Multilayered Orthotropic Plates," *Composite Structures*, Vol. 50, No. 2, 2000, pp. 183–198.

A. M. Waas
Associate Editor